O^- formation in grazing scattering from an Al(111) surface

C. Auth and H. Winter
Institut für Physik, Humboldt-Universität zu Berlin, Invalidenstrasse 110, D-10115 Berlin, Germany

A. G. Borisov, B. Bahrim, D. Teillet-Billy, and J. P. Gauyacq
Laboratoire des Collisions Atomiques et Moléculaires, (Unité de Recherche associée au CNRS D0281), Bâtiment 351, Université Paris-Sud, 91405 Orsay Cedex, France

(Received 9 October 1997)

We report on the results of a joint experimental and theoretical study on the formation of O^- ions in grazing scattering from an Al(111) surface. The O^- fractions in the scattered beam are studied over a wide range of collision energies. This allows us to observe a resonance structure for the O^- formation probability as a function of the collision velocity component parallel to the surface ($\mathbf{v}_\parallel$). Such a characteristic $\mathbf{v}_\parallel$ dependence is the signature of a kinematically induced charge-transfer process between the O^- ion and the Al surface. The theoretical treatment of charge transfer is based on the coupled angular mode method. The multistate aspect of the problem originating from the open-shell structure of the O^- ion is taken into account. [S0163-1829(98)00219-7]

I. INTRODUCTION

Negative-ion states are involved in quite a few phenomena occurring during atom/molecule interactions with metal surfaces. Stable negative ions can be formed during scattering or sputtering processes from solids.[1] In addition, they serve as intermediates in a variety of processes such as quenching of excited states,[2] vibrational excitation of adsorbed molecules,[3] reactive scattering,[4] and desorption of ions and neutrals.[5]

One of the specific properties of negative ions is the small binding energy of the active electron. Electron affinities of negative ions typically lie in the few eV range (e.g., 0.75 eV for H^-, 1.46 eV for O^-, and 3.4 eV for F^-). Then Auger capture processes can be ruled out and the negative-ion formation/destruction at metal surfaces is governed by the resonant electron transfer (RT) between metal and negative-ion states.

Detailed experimental studies have been devoted to the role of the RT process in negative-ion formation at clean and adsorbate-coated metal surfaces.[6–20] Due to the rather small binding energy, the affinity level of the negative ion is primarily in resonance with unoccupied electronic states of the surface above the Fermi level. Then the RT process is dominated by the neutralization of the negative ion via electron loss from the affinity level to the metal surface. As a result, small negative-ion fractions are formed at simple metal surfaces, with the exception of the negative halogen ions that can be efficiently formed at metal surfaces due to their relatively large electron affinities.[17] Two methods can be used to increase the negative-ion yield. One possibility consists in lowering the work function of the metal by alkali adsorption.[6,8–14] Another possibility, present in grazing scattering geometry, is the kinematically induced electron-transfer process, i.e., RT assisted by the collision velocity component parallel to the surface.[7,19,20] Detailed discussions on this so-called ''$\mathbf{v}_\parallel$ effect'' can be found in Refs. 21–23.

Recent developments of nonperturbative methods, treating the properties of negative-ion states in front of metal surfaces,[24–26] have provided the quantitative tools to study RT processes. One of these methods, the coupled angular mode (CAM) method, has been used to treat the O^- survival probability on surfaces with variable work functions[27] as well as the parallel velocity assisted H^- formation in grazing scattering at metal surfaces.[28] In both cases a quantitative agreement with the experimental results was obtained.

In this paper we report on an experimental as well as a theoretical study of O^- formation in grazing scattering at a metal surface. We use an Al(111) target, a prototype of the free-electron metal. Compared to a recent experimental study on O^- formation at an Au(110) surface,[19,20] a much larger energy range and a variation over scattering angles are encompassed in our study. Therefore, we are able to observe a ''resonant'' structure for the O^- formation probability as a function of the velocity component parallel to the surface. Image-charge-acceleration measurements provide complementary information on the O^- formation distances in addition to what can be deduced from the dynamical thresholds for the negative-ion formation.

From the theoretical point of view, the study of the dynamical resonant-transfer process involving the O^- ion and the O atom is quite elaborate. O^- (O) has an incomplete p-shell structure with five (four) $2p$-electrons that can *a priori* participate in the RT process. As discussed in Ref. 27, the O^- ion has a ^2P symmetry and can lose one of its $2p$ electrons to form the ground ^3P or metastable ^1D or ^1S states of the O atom in a $2p^4$ configuration. Together with the existence of different magnetic sublevels, this results in a multistate character of the problem that is further complicated by the $\mathbf{v}_\parallel$ effect on RT. To treat the dynamical RT process we use a multistate rate equation approach,[29] where the parallel velocity effects are incorporated via the ''shifted Fermi sphere'' model.[21–23,30] The inputs for the dynamical treatment are the static properties of an O^- ion in front of an Al

surface obtained with the CAM method. Finally, we describe the experiments and compare our experimental data with the theoretical studies for a wide range of scattering conditions ($v_\perp$, $v_\parallel$). Here $v_\perp$ stands for the velocity component normal to the surface.

II. THEORETICAL DESCRIPTION OF THE O^- FORMATION

A. Static properties of the O^- ion in front of the Al surface

We use the CAM method[25] to calculate the static properties of the O^- ion in front of the Al surface (energies of negative-ion states, partial decay rates into different channels, and angular distributions of the electrons ejected into the metal). Basically, one studies the electron scattering problem in the compound potential created by the metal surface and the oxygen atom in front of it. Negative-ion states appear as scattering resonances. We use a free-electron model to represent the Al metal and the effective range approach[31] to describe electron scattering by the O atom. For further details on the CAM treatment of the O^-/Al system we refer to an earlier publication.[27] Here, we briefly discuss static results with emphasis on the modifications introduced by the grazing angle geometry. The O^- ion corresponds to a ^2P symmetry. Three substates of different M_L (projection of the total orbital momentum on the quantization axis) are formed. The z axis normal to the surface and going through the ion center is chosen as the quantization axis to keep the cylindrical symmetry of the problem. The presence of the metal surface partly lifts the degeneracy of the M_L states. $M_L=0$ and $|M_L|=1$ states *a priori* are coupled to the surface differently and therefore have different energies and widths. The $M_L=1$ and $M_L=-1$ states are still degenerate.[27]

By losing one of its $2p$ electrons, the O^- ion can be neutralized in front of the surface. The neutral O atom has the stable configuration $1s^2 2s^2 2p^4$. From this, three states of ^3P, ^1D, and ^1S symmetry can be formed. ^3P and ^1D states have magnetic sublevels: $M_L=0, \pm 1$ and $M_L=0, \pm 1, \pm 2$, respectively. Depending on the O^- ion substate that is losing an electron, and on the spin and angular momentum of the detached electron, different O atom states can be formed. Similarly, the different substates of the O atom can capture a metal electron to form the different substates of the O^- ion.

At this point it should be stressed that, because of the different energies of the three neutral cores (^3P, ^1D, and ^1S), the O^- ion presents different binding energies with respect to its parents. The energy of the free O^- ion is $E_{^3P}=-1.46$ eV, with respect to the ^3P state of the O atom, $E_{^1D}=-3.43$ eV, with respect to the ^1D state of the O atom, $E_{^1S}=-5.65$ eV, with respect to the ^1S state of the O atom.

In the effective range approach, one uses an open-shell description of the O^- negative ion ($2p^4 2p'$) that allows an easy description of the three neutral core states and the three different binding energies of O^- with respect to the neutral channels. In this approach, the five O^- electrons are treated equivalently in the inner region close to the nuclei and in the outer region they are described as $2p^4 2p'$, the $2p'$ orbitals being different for the different neutral channels. The $2p'$ orbitals describe the loosely bound outer electron of O^- in the different channels and are thus the active orbitals in the RT process.

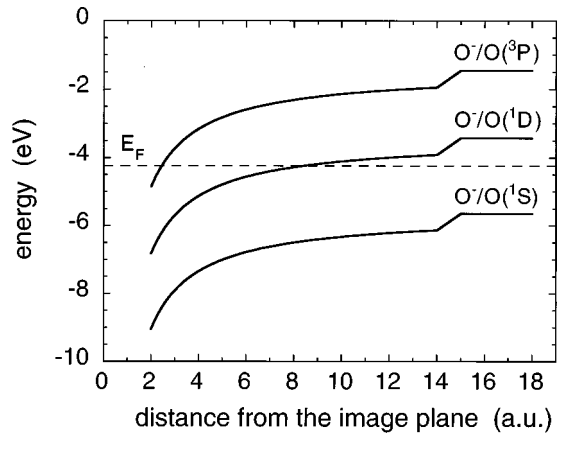

FIG. 1. Schematic energy positions of the O^- levels in front of an Al surface, with respect to three O(^3P, ^1D, and ^1S) states as functions of the atom-surface distance Z. The dashed horizontal line defines the position of the Fermi level.

In Ref. 27 the static properties (energy and width) of $O^-(M_L=0)$ and $O^-(|M_L|=1)$ states in front of the Al surface have been calculated by the CAM method. In front of the surface, the energy of the O^- ion is shifted by $\Delta E(Z)$ (Z is the ion-surface distance measured from the image plane). In a first approximation, this energy shift follows the image charge interaction: $\Delta E(Z)=-1/4Z$. However, when looking more closely, the M_L states are no longer degenerate and ΔE is slightly different for the $O^-(M_L=0)$ and $O^-(|M_L|=1)$ substates. Depending on the O atom state involved in O^- formation/destruction, different energies should be considered:

$$E_j^{|M_L|}(Z)=E_j+\Delta E^{|M_L|}(Z), \quad j=\{^3P,^1D,^1S\}. \tag{1}$$

In Fig. 1 we have sketched the energy positions of the O^- level in front of an Al(111) surface [$E_j^{|M_L|}(Z)$] with respect to the three states of the ground term of the neutral O atom (E_j). As an important feature, the O^- ion level lies below the Fermi level for all the decay channels at small atom-surface distances. However, there exists an intermediate range of distances where the ion level is above the Fermi level for the ^3P decay channel and below the Fermi level for the O excited-state channels. At these distances the O^- ion can be formed from the excited states and simultaneously decays into the O(^3P) channel, leading to a deexcitation process for the O singlet states (see, e.g., Ref. 27).

The total widths of the $O^-(M_L=0)$ and $O^-(|M_L|=1)$ states in front of the surface are different and roughly vary exponentially with the ion-surface distance. Results for the partial decay rates are summarized in Figs. 2(a), 2(b), and Table I. Note that the rates increase significantly from ^1S, ^1D to ^3P. The differences in the decay rates are mainly due to the difference in the binding energies of the O^- ion with respect to the corresponding O-atom states (see Fig. 1). Indeed, the probability of electron tunneling through the potential barrier separating the atom and the surface rapidly de-

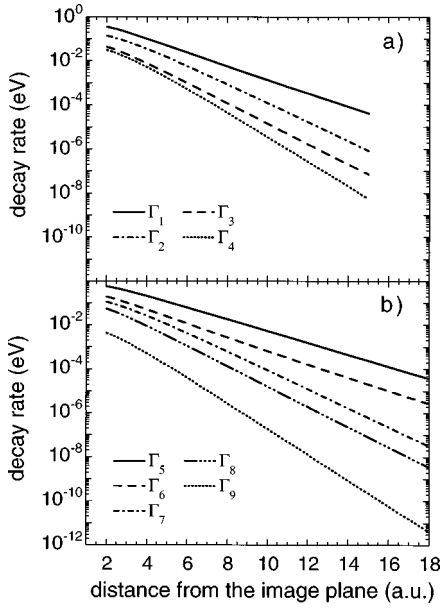

FIG. 2. Partial decay rates of the O^- substates for the various decay channels (see Table I) as functions of the ion-surface distance. (a) Decay rates of the O^- ($M_L=0$) substate; (b) decay rates of the O^- ($|M_L|=1$) substates.

creases when the binding energy of the tunneling electron increases. So the smallest binding energy (^3P channel) is associated with the largest partial decay rate, while the largest binding energy (^1S channel) is associated with the smallest partial decay rate. One can similarly account for the different slopes of the $\Gamma_1(Z)$ curves that are related to the energies of the transferred electrons. Further dependence of the decay rates on the magnetic substates involved in the transition is discussed in detail in Ref. 27.

In grazing scattering geometry, the only symmetry of the problem is that with respect to the scattering plane. Therefore the basis of M_L, m states, appropriate to treat the static problem of the O^- ion interacting with the surface, is not suitable for the treatment of the dynamics of the parallel velocity assisted charge transfer. The treatment of the dynamical RT by the ''shifted Fermi sphere'' model breaks the cylindrical symmetry around the z axis so that new symmetry-adapted states have to be considered (see Ref. 32 for more details). Indeed, the capture and loss rates obtained in a static study can still be used, when redefined in a proper basis. Symmetric and antisymmetric combinations have to be formed from the M_L, m states. We define the scattering plane as the (x,z) plane and the surface as the (x,y) plane. For the active electron, symmetric $|s\rangle$ and antisymmetric $|a\rangle$ combinations with respect to the (x,z) plane can be formed from the degenerate $m=\pm 1$ states as

$$|s_1\rangle=\frac{1}{\sqrt{2}}(|m=1\rangle-|m=-1\rangle)=|p_x\rangle,$$

$$|a_1\rangle=\frac{1}{\sqrt{2}}(|m=1\rangle+|m=-1\rangle)=|p_y\rangle, \tag{2a}$$

$$|s_0\rangle=|m=0\rangle=|p_z\rangle;$$

where the subscripts refer to the m manifold from which the symmetric or antisymmetric state is formed. $|p_x\rangle$, $|p_y\rangle$, and $|p_z\rangle$ stand for the electronic states oriented along the x, y, and z axis, respectively:

$$\langle \mathbf{r}|p_x\rangle=x\Psi(r),$$

$$\langle \mathbf{r}|p_y\rangle=y\Psi(r), \tag{2b}$$

$$\langle \mathbf{r}|p_z\rangle=z\Psi(r),$$

where $r=\sqrt{x^2+y^2+z^2}$. Under the reflection with respect to the (x,z) plane ($y\rightarrow -y$), the $|p_y\rangle$ orbital changes its sign (antisymmetric), while the $|p_x\rangle$ and $|p_z\rangle$ orbitals do not change their sign (symmetric).

In the same way, one can form symmetric and antisymmetric states of O and O^- from the proper combination of the M_L substates. For the $M_L=0$ states, by superposing the symmetry properties of the orbitals in the many electron wave functions, one can obtain the symmetry properties of the O^- and O states and we have the symmetric states $O^-(M_L=0)$, $O(^1S_{M_{L=0}})$, $O(^1D_{M_{L=0}})$, and the antisymmetric state $O(^3P_{M_{L=0}})$.

And for each of the degenerate $|M_L|\neq 0$ substates, symmetric and antisymmetric combinations are formed in a way similar to Eq. 2(a). One can then obtain the capture and loss rates for the symmetry-adapted states, using the proper spin and angular momentum statistical factors together with the partial decay rates presented in Figs. 2(a) and 2(b) and in Table I. The results for the capture and loss rates redefined in the new basis are given in Table II.

B. Time evolution of the charge states

In the case of grazing collisions, the kinematic effects smooth out the clear cut separation between occupied and unoccupied metal states.[21–23,30] In that sense the parallel velocity effect on the projectile-surface charge transfer is analogous to the effect of a very high temperature of the surface. For such conditions the population evolution of the projectile states can be described within a rate-equation approach.[33,34] Taking into account all the states that are involved, one can write.[29]

TABLE I. Partial decay rates of the $O^-(M_L=0)$ and $O^-(|M_L|=1)$ states. Γ_i corresponds to the decay rates into various decay channels (formation of O atom in ^3P, ^1D, or ^1S state). m is the projection of the angular momenta of the ejected electron on the quantization axis.

	^3P, $m=0$	^3P, $\lvert m\rvert=1$	^1D, $m=0$	^1D, $\lvert m\rvert=1$	^1S, $m=0$	^1S, $\lvert m\rvert=1$
$O^-(M_L=0)$	0	Γ_1	Γ_2	Γ_3	Γ_4	0
$O^-(\lvert M_L\rvert=1)$	Γ_5	Γ_6	Γ_7	Γ_8	0	Γ_9

TABLE II. Loss and capture rates for different O^-/O substrates with the proper symmetry with respect to the scattering plane. $O^-(S_1/A_1)$ represents the symmetric/antisymmetric state, formed from the $O^-(|M_L|=1)$ states, $O^-(S_0)$ represents the symmetric $O^-(M_L=0)$ state. $^3P(S_M,A_M)$, $^1D(S_M,A_M)$, and $^1S(S_0)$ represent the symmetric/antisymmetric states formed from the various $\pm M$ states of O atom (see text). s_1/a_1 represents the symmetric/antisymmetric state of the active $|m|=1$ electron [see Eq. (1)]. s_0 represents the ($m=0$) state of the active electron.

	$^3P(A_0)$	$^3P(A_1)$	$^3P(S_1)$	$^1D(S_0)$	$^1D(A_1)$	$^1D(S_1)$	$^1D(A_2)$	$^1D(S_2)$	$^1S(S_0)$
$O^-(S_0)$ loss	0	$\frac{1}{2}\Gamma_1,a_1$	$\frac{1}{2}\Gamma_1,s_1$	Γ_2,s_0	$\frac{1}{2}\Gamma_3,a_1$	$\frac{1}{2}\Gamma_3,s_1$	0	0	Γ_4,s_0
$O^-(S_0)$ capture	0	$\frac{1}{3}\Gamma_1,a_1$	$\frac{1}{3}\Gamma_1,s_1$	$2\Gamma_2,s_0$	Γ_3,a_1	Γ_3,s_1	0	0	$2\Gamma_4,s_0$
$O^-(A_1)$ loss	Γ_6,s_1	Γ_5,s_0	0	$\frac{1}{7}\Gamma_8,a_1$	Γ_7,s_0	0	$\frac{6}{14}\Gamma_8,s_1$	$\frac{6}{14}\Gamma_8,a_1$	Γ_9,a_1
$O^-(A_1)$ capture	$\frac{2}{3}\Gamma_6,s_1$	$\frac{2}{3}\Gamma_5,s_0$	0	$\frac{2}{7}\Gamma_8,a_1$	$2\Gamma_7,s_0$	0	$\frac{6}{7}\Gamma_8,s_1$	$\frac{6}{7}\Gamma_8,a_1$	$2\Gamma_9,a_1$
$O^-(S_1)$ loss	Γ_6,a_1	0	Γ_5,s_0	$\frac{1}{7}\Gamma_8,s_1$	0	Γ_7,s_0	$\frac{6}{14}\Gamma_8,a_1$	$\frac{6}{14}\Gamma_8,s_1$	Γ_9,s_1
$O^-(S_1)$ capture	$\frac{2}{3}\Gamma_6,a_1$	0	$\frac{2}{3}\Gamma_5,s_0$	$\frac{2}{7}\Gamma_8,s_1$	0	$2\Gamma_7,s_0$	$\frac{6}{7}\Gamma_8,a_1$	$\frac{6}{7}\Gamma_8,s_1$	$2\Gamma_9,s_1$

$$\frac{dP^i_{\text{ion}}}{dt}=-\left\{\sum_j G^{\text{loss}}_{ij}\right\}P^i_{\text{ion}}+\sum_j G^{\text{capt}}_{ij}P^j_{\text{neutral}},$$
$$\frac{dP^j_{\text{neutral}}}{dt}=-\left\{\sum_i G^{\text{capture}}_{ij}\right\}P^j_{\text{neutral}}+\sum_i G^{\text{loss}}_{ij}P^i_{\text{ion}}. \tag{3}$$

In Eq. (3) P^i_{ion} and P^j_{neutral} are the populations of the negative-ion and neutral atom substates defined in Table II,

$$i=\{O^-(S_0),O^-(A_1),O^-(S_1)\},$$
$$j=\{^3P(A_0),^3P(A_1),^3P(S_1),^1D(S_0),^1D(A_1),^1D(S_1),\times{}^1D(A_2),^1D(S_2),^1S(S_0)\}. \tag{4}$$

G^{loss}_{ij} and G^{capt}_{ij} are the electron loss and electron capture rates, respectively.

The effect of the parallel velocity is incorporated into the theoretical description by taking into account the frame transformation between the ion and the metal.[21–23,30] In the rest frame of the ion, the resonant transition rates are obtained from (θ, φ are the polar coordinates of the metal-state wave vector $\mathbf{k}$ with respect to the quantization axis)

$$\begin{Bmatrix} G^{\text{capt}}_{ij}(Z) \\ G^{\text{loss}}_{ij}(Z)\end{Bmatrix}=\begin{Bmatrix}\Gamma^{\text{capt}}_{ij}(Z)\\ \Gamma^{\text{loss}}_{ij}(Z)\end{Bmatrix}\int_0^{\pi/2}\sin\theta\, d\theta \times\int_0^{2\pi}d\varphi|\sigma^{\chi}_{ij}(\theta,\varphi,Z)|^2 \times\begin{Bmatrix} f\left(E_F-\dfrac{(\mathbf{k}_{ij}+\mathbf{v}_\parallel)^2}{2}\right)\\ 1-f\left(E_F-\dfrac{(\mathbf{k}_{ij}+\mathbf{v}_\parallel)^2}{2}\right)\end{Bmatrix}. \tag{5}$$

In Eq. 5, $\Gamma^{\text{loss}}_{ij}$ and $\Gamma^{\text{capt}}_{ij}$ are the ''static'' capture and loss rates presented in Table II. $|\sigma^{\chi}_{ij}(\theta,\varphi,Z)|^2$ describes the angular distribution for the probability of electron transfer between the O^- ion and the metal.[28] χ refers to the state of the active electron: $\chi=\{s_0,s_1,a_1\}$. This angular distribution function is normalized as

$$\int_0^{\pi/2}\sin\theta\, d\theta\int_0^{2/\pi}d\varphi|\sigma^{\chi}_{ij}(\theta,\varphi,Z)|^2=1. \tag{6}$$

The angular distribution $|\sigma^{\chi}_{ij}(\theta,\varphi,Z)|^2$ corresponds to the atomic states with the proper symmetry with respect to the scattering plane. Details on this point are discussed in Ref. 32. $f(E_F-(\mathbf{k}_{ij}+\mathbf{v}_\parallel)^2/2)$ is the ''Fermi-Dirac'' function (E_F is the Fermi energy) in the rest frame of the moving ion. This is affected in a characteristic way by the motion parallel to the surface (''shifted Fermi sphere'' model[23,30]) and for a vanishing temperature can be expressed by the step-function Θ ($\mathbf{v}_\parallel$ along the x axis):

$$f\left(E_F-\frac{(\mathbf{k}_{ij}+\mathbf{v}_\parallel)^2}{2}\right)=\Theta\left(E_F-\frac{k_{ij}^2+v_\parallel^2}{2}-v_\parallel k_{ij}\sin\theta\,\cos\varphi\right), \tag{7}$$

where $k_{ij}\equiv|\mathbf{k}_{ij}|$ is fixed by the resonance condition

$$k_{ij}=\sqrt{2(U_0-E_{ij})}. \tag{8}$$

U_0 is the bottom of the conduction band (jellium metal). E_{ij} is the binding energy of the electron in the ith state of the O^- ion with respect to jth channel. It is obtained from Eq. (1).

Equation (3) is integrated numerically along the outgoing path of the scattered particle. The trajectory is assumed to be a straight line followed with constant velocity. The starting point of the integration Z_{ini} was taken equal to 2 a_0 (measured from the image plane). For such a short distance, the final population of the various states does not depend on the initial populations at Z_{ini}. Indeed, close to the surface the rates for the RT process are high. Any memory of the initial populations is quickly erased and the system relaxes towards a local equilibrium population given by the competition between loss and capture rates in Eq. (3). However, as Z_{ini} increases, the final population becomes dependent on the initial conditions.

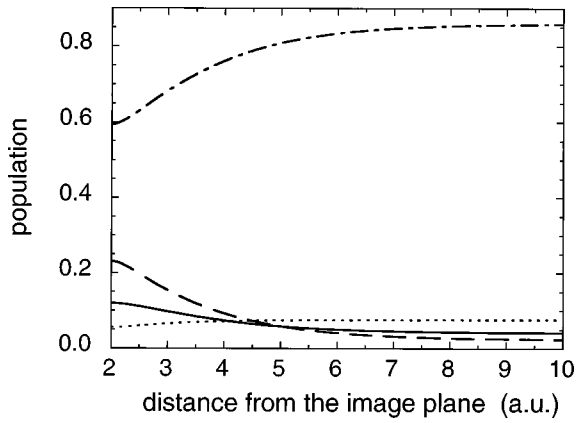

FIG. 3. Populations of the various states as functions of the projectile-surface distance in the outgoing trajectory path. The exit angle is 1.8° with respect to the surface and the collision velocity is equal to 0.2 a.u. The integration of the rate equations is started at $Z_{\text{int}}=2\,a_0$ with the initial populations of different states equal to their equilibrium values for this velocity. Solid line, $O^-(S_0)$ substate; dashed line, summed population of the $O^-(S_1)$ and $O^-(A_1)$ substates; dashed-dotted line, total $O(^3P)$ ground-state population; dotted line, total $O(^1D)$ excited-state population.

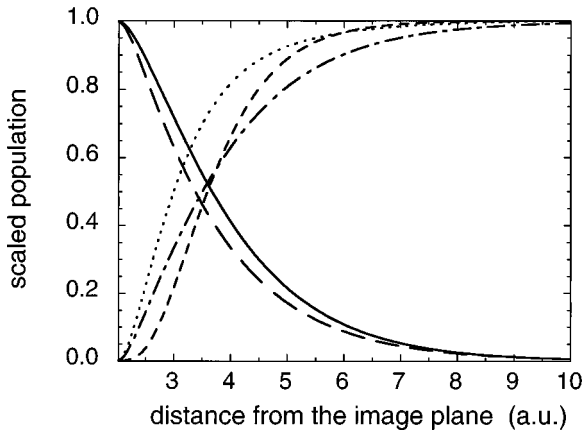

FIG. 4. Scaled populations of various states as functions of the projectile-surface distance, for the same case as in Fig. 3. Solid line $O^-(S_0)$ substate; long-dashed line, summed population of the $O^-(S_1)$ and $O^-(A_1)$ substates; dashed-dotted line, total $O(^3P)$ ground-state population; dotted line, total $O(^1D)$ excited-state population; short-dashed line, total $O(^1S)$ excited-state population.

When several states are involved in the charge-transfer process, their population dependence on the atom-surface distance, collision velocity, and the properties of the surface (work function) is rather complicated. Certain states, even if they are not populated *at the end of the collision*, can exist as transient states *during the collision* and thus deeply influence the final populations of the other states.[2,11,14,35–37] In Fig. 3 we present the time evolution of the populations of the various states as functions of the atom-surface distance when the oxygen atom leaves the surface (the ^1S population being too small is not shown on the figure). It corresponds to scattering conditions typical of the experimental study: an exit angle of 1.8° with respect to the surface and a collision velocity equal to 0.2 a.u. (16 keV collision energy, and 16 eV perpendicular energy). The integration of the rate equations is started at $Z_{\text{ini}}=2a_0$ with the initial populations of different states equal to their equilibrium values for this velocity. For a given projectile-surface separation, the local equilibrium values of P^i_{ion} and P^j_{neutral} are such that the right-hand sides of Eq. (3) are equal to zero.

As the projectile recedes from the surface, the ion population decreases in favor of the neutral states as a consequence of the variation of the ionic level energy with the atom-surface distance. Most of the population variation occurs in the 3–5 a_0 range. In order to stress the large distance variation, Fig. 4 presents scaled populations as functions of Z. For the neutral states they are defined as

$$P^{\text{scaled}}=\frac{P(Z)-P(Z=2)}{\text{Max}[P(Z)-P(Z=2)]},$$

and for the ion states,

$$P^{\text{scaled}}=\frac{P(Z)-P(\infty)}{\text{Max}[P(Z)-P(\infty)]}.$$

The neutral state populations are seen to stabilize at different atom-surface distances: the ^1S population reaches its asymptotic value earlier than the ^1D population and the ^3P population is the last one to reach its asymptote. The ion population reaches its asymptote at the same time as the ^3P level. The difference between the various stabilization distances has to be linked with the difference between the various transition rates (see Fig. 2). Indeed, the ^1S state is associated with the smallest partial width, with the largest slope as a function of Z, and is thus associated with the fastest convergence of its population when Z increases, or equivalently to the smallest distance of the final charge state formation (''freezing distance''[38]). However, because of the width of the freezing regions, one does not see on Figs. 3 and 4 the successive decoupling of the negative ion from the neutral states. On Fig. 4, the ion population is seen to quickly decrease as Z increases; as said above, this is due to the decrease of the equilibrium population of the ion level, a consequence of the variation of the ion level energy. The ionic population is seen to stabilize in the 5–9 a_0 distance range that can be considered then as an estimate of the so-called ''freezing distance.'' In the present case, the multistate character of the process associated with different distance domains makes difficult a more exact determination of the distance of final formation of the negative ion states. As is seen in the figure, the oxygen ground-state (^3P) population stabilizes in the same region of distances as the negative-ion population. That reflects the fact that, owing to its large width, the ^3P state dominates the charge transfer and basically determines the final O^- population. Furthermore, the excited states of the neutral atom correspond to large affinities, so that capture of electrons by the excited states is effective even at large distances. In contrast, the ^3P level very quickly crosses the Fermi level, so that the O^- ion can decay to form the oxygen ground state. As a consequence, any excited state population will be pumped down to the ground state due to the quenching process: $O(^1S,^1D)\rightarrow O^-\rightarrow O(^3P)$ (see also Ref. 27). So, for small parallel velocities, the excited-state population is very weak and the ^3P

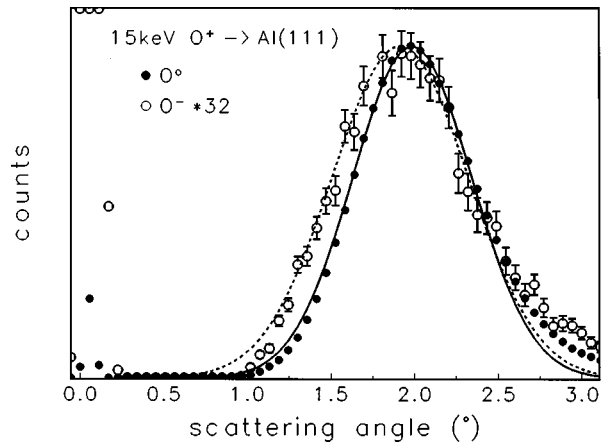

FIG. 5. Angular distributions of the scattered neutral oxygen atoms (full dots) and O^- ions (open circles) for 15 keV O^+ ions impinging on an Al(111) surface. The dashed and solid lines represent Gaussian fits to the O^- and O^0 angular distributions, respectively. The saturated signal at the zero angle corresponds to the incident beam.

state is dominating. However, the parallel velocity effect makes possible the formation of excited states and indeed the fraction of excited states in the beam increases with the parallel velocity (see Sec. IV).

III. EXPERIMENT

Oxygen atoms or ions with energies ranging from 1.5 to 700 keV (velocities $0.1 \leqslant v \leqslant 1.3$ a.u.) produced by a small accelerator equipped with an electron-cyclotron-resonance (ECR) -ion source are scattered after collimation (angular width $\delta\Phi < \pm 0.02°$) from a clean and flat Al(111) surface under a grazing angle of incidence $\Phi_{in} < 2°$. The experiments are performed in an UHV-scattering chamber at a pressure of about 10^{-10} mbar. Sets of electric field plates upstream and downstream with respect to the target are used to disperse the incoming and, in particular, the scattered beams with respect to charge states.

Special attention is paid to the demand of equal detection efficiencies for particles in different charge states, in particular for neutral O atoms and O^- ions. This is achieved by a thin carbon foil ($< 5\ \mu g/cm^2$) mounted on the entrance aperture of our channeltron (VALVO X919BL) detector. The charge state equilibrium is reached during the passage of projectiles through the foil in only a few atomic layers. This guarantees the same detection efficiency irrespective of the charge state of the incoming atomic particle.

The target surface is prepared by a large number of cycles by grazing sputtering with 25 keV Ar^+ ions and subsequent annealing of the target for about 5 min at a temperature of about 500 °C. In the final state of preparation we obtain defined angular distributions of scattered projectiles. A comparison with former investigations by SPALEED (spot profile analysis low energy electron diffraction) indicates a mean width of terraces formed by topmost surface atoms of typically 1000 a.u.[39]

As an example we present in Fig. 5 angular distributions after the scattering of 15 keV O^+ ions from the Al(111) surface. The two distributions shown are for projectiles that emerge from the surface as neutral atoms (full circles) and as negative ions (open circles), respectively.

The separation of the data with respect to charge states is achieved by applying a ''difference'' method,[40] where the data are recorded with biased (only neutral projectiles) and unbiased (all projectiles) electric-field plates, and the contributions of ions are obtained from the difference of the two data sets. For velocities $v < 0.5$ a.u., one charged component in the scattered beam dominates the charge spectra, so the difference of the two data sets gives directly the contribution of the negative ions. For higher velocities charge-state distributions are recorded by selecting part of the projectiles in the maximum of the scattering distribution with a slit and dispersing it with an electric field with respect to all charge states.

The data shown in Fig. 5 are arbitrarily normalized to the same heights of the maxima; i.e., the data for O^- ions are multiplied in this respect by a factor of 32. This means that the fraction of negative ions is 3% for this case. In comparing the two distributions, a slight shift of the data for ions towards smaller angles of scattering can be seen that is in particular evident for smaller angles of the distributions. Such an angular shift has been observed already in a number of studies for different sorts of atoms and their positive ions. It is attributed to the attractive image force acting on charged particles on the outgoing trajectories. From the angular shift one can estimate the distance of the final charge-state formation,[40,41] though, owing to the multistate aspect of the charge-transfer process, it is not a well-defined quantity in the present case. For the data shown here we get from fits with a Gaussian line shape a shift $\Delta\Phi = 0.08° \pm 0.03°$; this corresponds to an image-interaction energy $E_{im} = -(0.70 \pm 0.25)$ eV. We will comment on this result below.

A further aspect of the data displayed in Fig. 5 is related to measurements of ion fractions. Since the forces owing to image-charge interaction on ions affect the angular distributions particularly for subspecular angles of scattering, negative-ion fractions derived at those angles are clearly enhanced in comparison to the actual values derived from the intensities at the maxima or from an integration of the curves. Thus data at low energies ($E \leqslant 50$ keV) have to be recorded and analyzed taking into account image charge effects in order to avoid artificial enhancement of the negative ion fractions.

In Fig. 6 we present the negative-ion fractions as a function of the projectile velocity for the scattering of O atoms with various angles of incidence $\Phi_{in} = 0.63°$, 1°, and 1.8°. The data reveal the expected structure of a kinematic resonance with a threshold at $v_{th} \approx 0.1$ a.u. and a maximum at $v_{max} \approx 0.35$ a.u. The symbols represent the experimental data and the curves the results of our calculations with the model outlined in Sec. II. (Note the different scales for the theoretical and experimental results.) In Fig. 7 we show an enlarged view of the range of velocities around the threshold for ion formation (scattering angle 0.6°). No scaling factor is applied here. As is seen from Fig. 6, the ion fraction increases with the angle of incidence, i.e., with the collision velocity component normal to the surface, while exhibiting the same shape of the resonance curve. This variation is similar to the one observed for H^- formation,[28] and is easily explained in the freezing distance approximation: as the perpendicular velocity increases, the freezing distance decreases, and since the equilibrium ion population increases at small Z, this

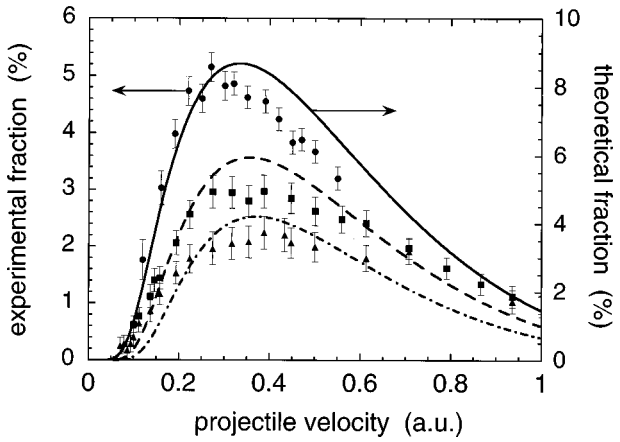

FIG. 6. Negative-ion fractions as functions of the projectile velocity for the scattering of O atoms from an Al(111) surface with various angles of incidence (Φ_{in}). The symbols represent the experimental data and the curves represent the theoretical results. Note the different scales for the experimental and theoretical results. Triangles and dashed-dotted line, $\Phi_{in}=0.63°$; squares and dashed line $\Phi_{in}=1°$; full dots and solid line, $\Phi_{in}=1.8°$.

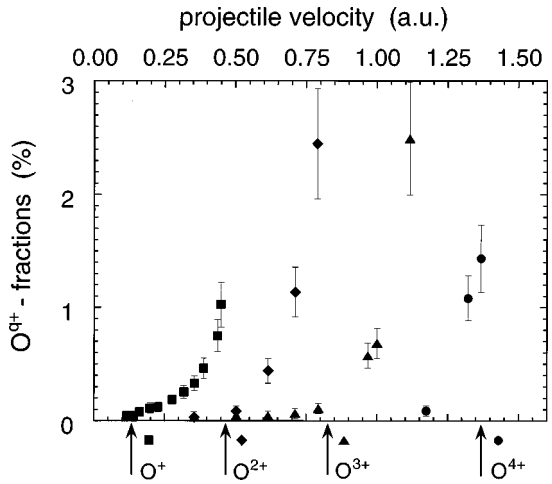

FIG. 8. Experimentally measured fractions of O^{q+} ions as functions of the projectile velocity after scattering from an Al(111) surface with an angle of incidence $\Phi_{in}=0.35°$. The arrows indicate the kinematic thresholds for the various Auger ionizations. Squares O^+ fraction; diamonds, O^{2+} fraction; triangles, O^{3+} fraction; filled circles, O^{4+} fraction.

leads to the observed variation. From Fig. 6 we can see that the theoretical ion fractions are higher than the experimental ones by a factor of about 1.6 at the maximum, although the general shape of the resonant curve is well reproduced. In the same time the agreement between theory and experiment is fairly good in the threshold region (Fig. 7). At this point we should stress that the theoretical approach is free from adjustable parameters. A discussion on possible origins for the discrepancy between experiment and theory results is presented in the next section.

Additional information for the interpretation of the data might be deduced from the appearance of positive ions in the scattered beams. The fractions of O^+ ions as functions of the projectile velocity are presented in Fig. 8. The data show a pronounced increase of the O^+ fractions for velocities $v \geqslant 0.1$ a.u.

Finally, we note that measurements on the energy loss of scattered projectiles show an energy loss smaller than 2.5% from the total energy. Thus the reduction of projectile velocities during the scattering from the surface can be neglected for the theoretical description even if the formation of O^- ions takes place on the outgoing path of the trajectory.

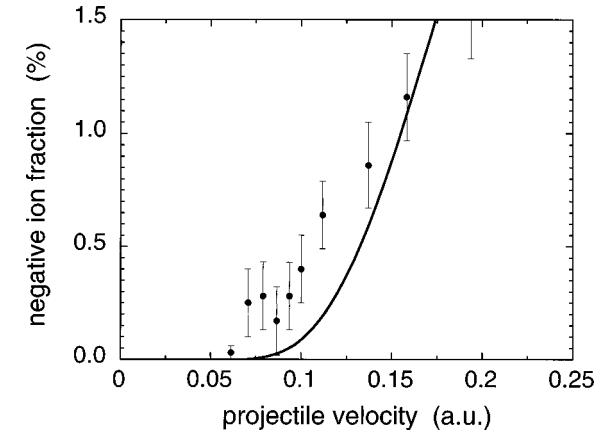

FIG. 7. Negative-ion fraction as a function of the projectile velocity for the scattering of O atoms from an Al(111) surface with an angle of incidence $\Phi_{in}=0.63°$. The full dots represent the experimental data and the solid line the theoretical results.

IV. DISCUSSION

We begin the discussion of our results with an analysis of the angular shift observed in the angular distributions shown in Fig. 5. Since the final formation of the O^- ions proceeds at a relatively large distance from the surface, one can describe the image potentials to a good approximation by the classical $1/4Z$ dependence. Then we deduce from the measured $E_{im} = -(0.70 \pm 0.25)$ eV a mean distance of final formation $Z_S = (9.7^{+5}_{-2.5})$ a.u. The relatively large uncertainties are due to the smallness of the O^- fractions and the widths of the angular distributions, which makes the application of the experimental method rather difficult (see previous section). Despite these problems, we can conclude that the final formation of O^- ions proceeds in an interval of distances that is located at about 10 a.u. from the image reference plane. This distance is significantly larger than $Z_S = 3$ a.u. as reported for the O^- formation at a Au surface by Meyer and co-workers.[19,20] Our estimate for the final O^- formation distance can be compared with the results presented in Figs. 3 and 4. Indeed, the ''final formation distance'' obtained from the angular shift should correspond to the distance where the coupling between the ion and neutral states disappears, i.e., to the distance where the populations stabilize at their asymptotic value. The region around $5-9a_0$ seen in Fig. 4 is consistent with the experimental finding. It should be stressed that in the present multistate problem, the couplings between the various ion and neutral states disappear in different broad and overlapping regions of atom-surface distances. So one cannot find a unique well-defined ''final formation distance'' for the O^- ion but rather a broad ''final formation zone.'' This effect is possibly the origin for the rather broad angular distributions seen in Fig. 5.

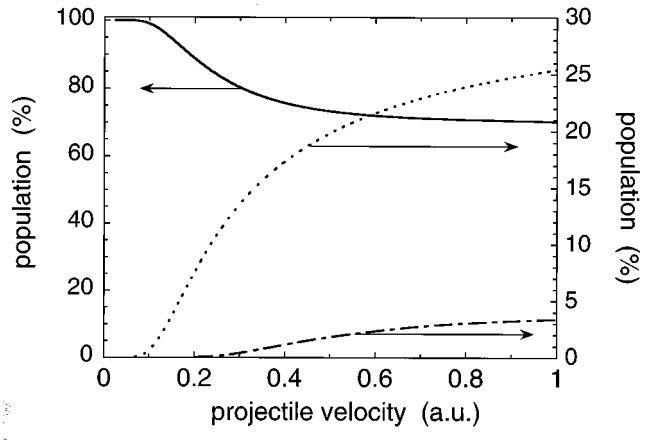

FIG. 9. Theoretical results for the final populations of the different O-atom states as functions of projectile velocity for scattering from an Al(111) surface with an angle of incidence $\Phi_{in}=1°$. Solid line, O(^3P) ground-state population; dotted line, O(^1D) excited-state population; dashed-dotted line, O(^1S) excited-state population.

The kinematic resonant structure observed for the O^- fractions as functions of the projectile velocity can be qualitatively understood by a frame transformation between the moving projectile and the metal surface. Then in the rest frame of the projectiles, the electronic conduction-band states of the metal appear modified (Galilei transformation), resulting in a ''Doppler-Fermi-Dirac distribution''[23,30] of occupied and empty electronic states. As a consequence of this kinematic effect, occupied metal states are brought into resonance with the affinity level of the ion, and negative ions can be formed via a resonant electron transfer. For this kinematically induced resonant-transfer process, we have characteristic velocities, as, e.g., the threshold of electron capture from the surface v_{th} and the velocity v_{max} for the highest probability of electron capture.[28,32] As can be seen from comparisons of the experimental data with the calculations, these kinematic structures for the O^- formation are well reproduced. In this respect it is interesting to note that the data sets presented in Fig. 6 are in overall good agreement with the calculations, if the theoretical O^- fractions are reduced by a common factor of about 1.6.

Our calculations predict that aside from negative ions and ground-state neutrals a significant population of excited states is present in the scattered beam. The excited-state fractions are presented in Fig. 9 as functions of the parallel velocity (incidence angle 1.8°). Note the different scales for the different states. For a vanishing parallel velocity, the quenching process (see Sec. II B) is very efficient and the neutral atoms are all formed in the ground state. However, as the velocity increases, the kinematic effect results in the existence of *both* capture and loss processes between the O^- ion states and the excited states of the O atom and leads to a significant population of excited states (around 30%) at large velocities.

The quantitative agreement between the experimental and theoretical results for O^- formation at an Al(111) surface is poorer than the one obtained with the same methods in other collisional systems: H^- ion formation and alkali ion neutralization on Al(111).[28,32] Possible explanations are examined below.

(1) In the present theoretical approach, the e^--O interaction is modeled by the approximation of effective range theory (ERT).[25,27] This introduces an uncertainty in the theoretical results. However, this description has been successfully used to study e^--O collisions,[31] so that one cannot *a priori* expect large errors owing to the use of the ERT approach.

(2) Another possibility could be the presence of transitions other than the O/O^- charge transfer. Indeed, the experimental results show the ionization of the O atom and even the formation of O^{+q} multicharged ions (Fig. 8). Figure 8 also displays the thresholds for the successive ionizations of O atoms via the kinematically induced Auger ionization process.[42–44] The observed thresholds support the idea that the kinematically induced Auger process might be responsible for the ionization of projectiles. The existence of the ionization process can influence the O^- formation if both processes occur in overlapping atom-surface distance ranges. This is not unlikely, since, as said above, we found that the independence of the final O^- population on the initial populations of different substates is only reached for rather small distances ($Z_{ini}\sim 2a_0$) and so, though ionization processes concern inner orbitals and are likely only close to the surface, they could in principle influence the final O^- formation. It should, however, be stressed that a very large perturbation of the system at small Z is required to modify the final ion fractions by a factor of 1.6.

(3) Finally, in the present approach, the O^- electrons are considered to be nonequivalent with the outer $2p'$ electrons and four inner $2p$ electrons, forming a ^3P, ^1D, or ^1S core. This corresponds to the $2p^4 2p'$ configuration of the O^- ion. As a consequence, electron transfer to/from the metal concerns only the outer $2p'$ electron; the transitions of the inner electrons are neglected. This description is based on the fact that the outer-electron binding energy (the O^- affinity) is much smaller than the binding energy of the inner electrons (typically the O ionization energy). This approximation works very well in the case of H^-; however, it could be poorer in the case of O^-. Indeed, the ratio between the ionization energy and affinity is about 10 for oxygen, while it is about 18 for hydrogen. Studies on halogen negative-ion formation in interactions with an Al(111) surface are currently in progress.[45] In this case the ratio between ionization energy and affinity of the projectile is even smaller. Preliminary results support our interpretation of the discrepancy between experimental and theoretical results as caused by the nonequivalent electron description of the O^- ion.

V. CONCLUSIONS

We have reported on a joint theoretical and experimental study of the O^- ion formation in grazing collisions on an Al(111) surface. O^- ions are formed by a resonant electron-capture process assisted by the collision velocity. The study has been performed over a wide range of collision energies, showing the complete resonance curve associated with the dynamical electron capture. The open shell structure of oxygen leads to a complex charge-transfer process involving all the ion and neutral states. This aspect is revealed by the

theoretical study showing how the different states participate in the process. An interesting consequence of the multistate character of the charge transfer is the population of excited neutral states in the scattered beam at large velocities. The results of the experimental and theoretical studies are found in good qualitative agreement; however, they differ by a general factor of about 1.6. A few origins for these differences have been discussed. The most probable is the ''nonequivalent electron'' description of the oxygen negative ion in the present theoretical approach.

[1] J. Ishikawa, in *Handbook of Ion Sources*, edited by B. Wolf (CRC, Boca Raton, 1995), p. 289.
[2] R. Hemmen and H. Conrad, Phys. Rev. Lett. **67**, 1314 (1991).
[3] J. E. Demuth, D. Schmeisser, and Ph. Avouris, Phys. Rev. Lett. **47**, 1166 (1981).
[4] L. Hellberg, J. Strömquist, B. Kasemo, and B. I. Lundquist, Phys. Rev. Lett. **74**, 4742 (1995).
[5] L. Sanche, J. Phys. B **23**, 1597 (1990).
[6] J. N. M. van Wunnik, J. J. C. Geerlings, and J. Los, Surf. Sci. **131**, 1 (1981); H. M. van Pixteren, C. F. A. van Os, R. M. A. Heeren, R. Rodink, J. J. C. Geerlings, and J. Los, Europhys. Lett. **10**, 715 (1989).
[7] R. Zimny, H. Nienhaus, and H. Winter, Nucl. Instrum. Methods Phys. Res. B **48**, 361 (1990).
[8] H. Brenten, H. Müller, K. H. Knorr, D. Kruse, H. Schall, and V. Kempter, Surf. Sci. **243**, 309 (1991).
[9] C. C. Hsu, H. Bu, A. Bosetta, J. W. Rabalais, and P. Nordlander, Phys. Rev. Lett. **69**, 188 (1992).
[10] E. R. Behringer, D. R. Andersson, B. Kasemo, B. H. Cooper, and J. B. Marston, Nucl. Instrum. Methods Phys. Res. B **78**, 3 (1993).
[11] E. R. Behringer, D. R. Andersson, B. H. Cooper, and J. B. Marston, Phys. Rev. B **54**, 14 765 (1996).
[12] Q. B. Lu, D. J. O'Connor, B. V. King, and R. J. MacDonald, Surf. Sci. **347**, L61 (1996).
[13] Q. B. Lu, R. Souda, D. J. O'Connor, B. V. King, and R. J. MacDonald, Phys. Rev. B **54**, R8389 (1996).
[14] C. B. Weare and J. A. Yarmoff, Surf. Sci. **348**, 359 (1996).
[15] M. Maazouz, L. Guillemot, T. Schlatholter, S. Ustaze, and V. A. Esaulov, Nucl. Instrum. Methods Phys. Res. B **125**, 283 (1997).
[16] V. A. Esaulov, O. Grizzi, L. Guillemot, M. Maazouz, S. Ustaze, and R. Verucci, Surf. Sci. **380**, L251 (1996).
[17] S. Ustaze, L. Guillemot, R. Verucci, and V. A. Esaulov, Surf. Sci. (to be published).
[18] C. A. Keller, A. C. Lavery, and B. H. Cooper (unpublished).
[19] F. W. Meyer, L. Folkerts, and S. Schippers, Nucl. Instrum. Methods Phys. Res. B **100**, 366 (1995).
[20] L. Folkerts, S. Schippers, D. M. Zehner, and F. W. Meyer, Phys. Rev. Lett. **74**, 2204 (1995).
[21] J. J. C. Geerlings and J. Los, Phys. Rep. **190**, 133 (1990).
[22] R. Brako and D. M. Newns, Rep. Prog. Phys. **52**, 655 (1989).
[23] J. N. M. van Wunnik, R. Brako, K. Makoshi, and D. M. Newns, Surf. Sci. **126**, 618 (1983).
[24] P. Nordlander, Phys. Rev. B **46**, 2584 (1992).
[25] D. Teillet-Billy and J. P. Gauyacq, Surf. Sci. **239**, 343 (1990).
[26] V. A. Ermoshin and A. K. Kazansky, Phys. Lett. A **218**, 99 (1996).
[27] B. Bahrim, D. Teillet-Billy, and J. P. Gauyacq, Phys. Rev. B **50**, 7860 (1994); Surf. Sci. **316**, 189 (1994).
[28] A. G. Borisov, D. Teillet-Billy, and J. P. Gauyacq, Surf. Sci. **278**, 99 (1992).
[29] D. C. Langreth and P. Nordlander, Phys. Rev. B **43**, 2541 (1991).
[30] D. M. Newns, Comments Condens. Matter Phys. **14**, 295 (1989).
[31] D. Teillet-Billy and J. P. Gauyacq, J. Phys. B **22**, L335 (1989).
[32] A. G. Borisov, D. Teillet-Billy, J. P. Gauyacq, H. Winter, and G. Dierkes, Phys. Rev. B **54**, 17 166 (1996).
[33] J. J. C. Geerlings, J. Los, J. P. Gauyacq, and N. M. Temme, Surf. Sci. **172**, 257 (1986).
[34] R. Brako and D. M. Newns, Surf. Sci. **108**, 253 (1981).
[35] S. Schipers, S. Oelschig, W. Heiland, L. Folkerts, R. Morgenstern, P. Eeken, I. F. Urazgil'din, and A. Niehaus, Surf. Sci. **257**, 289 (1991).
[36] H. Brenten, H. Müller, and V. Kempter, Surf. Sci. **271**, 103 (1992).
[37] J. B. Marston, D. R. Andersson, E. R. Behringer, B. H. Cooper, C. A. DiRubio, G. A. Kimmel, and C. Richardson, Phys. Rev. B **48**, 7809 (1993).
[38] E. G. Overbosch, B. Rasser, A. D. Tenner, and J. Los, Surf. Sci. **92**, 310 (1980).
[39] G. Dierkes, Diploma thesis, Münster, 1993.
[40] H. Winter, Phys. Rev. A **46**, R13 (1992).
[41] H. Winter, J. Phys.: Condens. Matter **8**, 10 149 (1996).
[42] R. Zimny and Z. L. Miskovic, Nucl. Instrum. Methods Phys. Res. B **58**, 387 (1991).
[43] R. Zimny, Z. L. Miskovic, N. N. Nedeljkovic, and Lj. D. Nedeljkovic, Surf. Sci. **255**, 135 (1991).
[44] H. Winter, Nucl. Instrum. Methods Phys. Res. B **78**, 38 (1993).
[45] A. G. Borisov, D. Teillet-Billy, G. P. Gauyacq, A. Mertens, C. Auth, and H. Winter (unpublished).